Non-reactive scattering of N_2 from the W(110) surface studied with different exchange-correlation functionals

K.R. Geethalakshmi,[1,2,*] J.I. Juaristi,[1,2,3,†] R. Díez Muiño,[1,2,‡] and M. Alducin[1,2,§]

[1] *Centro de Física de Materiales (CSIC-UPV/EHU) - Materials Physics Center MPC, P. Manuel de Lardizabal 5, 20018 San Sebastián, Spain*

[2] *Donostia International Physics Center DIPC, P. Manuel de Lardizabal 4, 20018 San Sebastián, Spain*

[3] *Departamento de Física de Materiales, Facultad de Químicas, Apartado 1072, 20080 San Sebastián, Spain*

Abstract

The non-reactive scattering of N_2 from the W(110) surface is studied with six dimensional (6D) classical dynamics and two distinct potential energy surfaces (PES). Here, we use the PESs calculated with density functional theory and two different exchange-correlation functionals, the PW91 [J. E. Perdew *et al.*, Phys. Rev. B **46**, 6671 (1992)] and the RPBE [B. Hammer *et al.*, Phys. Rev. B **59**, 7413 (1999)]. By analyzing the final rotational state and angular distributions, we extract information on the characteristics of the two PESs in the 6D configurational space. Comparison of the theoretical results with the available experimental data provides detailed information on the validity of each functional. In general, the PW91 PES is more corrugated than the RPBE one in all the configurational space, meaning that there is a stronger dependence of the potential energy on the molecular orientation and position over the surface unit cell. Furthermore, we find that the larger corrugation and the less repulsive character exhibited by the PW91 PES seems to be realistic at distances above the chemisorption well. In contrast, the less corrugated RPBE PES performs better in the region below the chemisorption well.

I. INTRODUCTION

In the numerical simulations of the interaction of diatomic molecules impinging on metal surfaces the problem is usually split in two parts. First, the six-dimensional (6D) potential energy surface (PES) for the molecule-surface interaction is obtained. Second, on top of this PES, classical or quantum mechanical dynamics are performed. As a consequence, the accuracy of this approach to simulate the molecule-surface interaction relies on the quality of the PES.

State-of-the-art PESs are usually obtained from the interpolation of ab-initio density functional (DFT) energies calculated for a set of different molecule-surface configurations. DFT is an exact theory that loses its accuracy in practice due to the unknown form of the exchange-correlation (XC) functional to be used in the Kohn-Sham scheme. In this respect, the generalized gradient approximation (GGA) in which the XC energy is a functional of both the electronic density and its gradient, is the standard accurate gas/surface description employed in this kind of calculations. Since there are different GGAs available, an analysis of how the theoretical predictions are affected by the choice of the XC functional provides information on the level of accuracy that can be achieved. The dynamics of H_2 on metal surfaces is one of the benchmarks that has been used to check the accuracy of two widely used functionals, the PW91[1] and the RPBE[2]. In general, it is observed that the reactivity predicted with the PW91 functional is significantly higher than the values obtained with the RPBE[3–5]. Díaz *et al.*[5] proposed a mixture between both functionals to achieve accuracies in the order of ∼4.2 kilojoules per mole, when simulating the dynamics of thermal H_2 on Cu(111). The limitations of present GGAs to predict the reactivity of thermal molecules remain when dealing with heavier molecules. In ref. 6, it has been presented a comparison between the theoretical predictions for the dissociative adsorption of N_2 on different tungsten surfaces, when using PESs calculated with the PW91 and RPBE functionals. It was shown that the results for the dissociative adsorption probability with the two PESs differ significantly. In fact, these differences can be larger than the ones obtained between adiabatic and non-adiabatic calculations that include the effect of electronic friction in the dissociation process[7]. Comparison with the dissociative probabilities measured in molecular beam experiments[8–13] for different incident energies and different incidence angles of the impinging molecules did not lead to a definite conclusion as to which functional provides

the better PES. The reason is that each functional performed better for different initial conditions. Briefly, it was concluded that the RPBE functional appeared to produce a too repulsive PES far from the surface, thought it seemed to describe better than the PW91 the regions close to the chemisorption well.

A limitation in extracting information uniquely from the obtained results for the dissociative adsorption probability is that the final state of the dissociation process is not directly accessible in the simulations. In fact, the final state of the dissociating molecule corresponds to two nitrogen atoms with large internuclear distance (around twice the equilibrium internuclear distance) and positive radial velocity. These nitrogen atoms still have large kinetic energies that will be subsequently dissipated as they diffuse on the surface until they are stabilized on the equilibrium adsorption sites. Therefore, the final state of the adsorbates accessible to experiments is determined by this energy dissipation mechanism and does not give direct information about the dissociation process that is simulated in order to calculate the dissociative adsorption probabilities. This limitation disappears if one analyzes the dynamics of the scattered molecules for which the simulated final state is also accessible experimentally, what allows a more direct comparison between theory and experiment.

In this work, we use both the PW91 and RPBE PESs to study the non-reactive scattering of N_2 on the W(110) surface. Results from the angular distribution of the reflected molecules and their rotational state population distributions are presented. These scattering distributions have been measured for a variety of molecule-surface systems[14–28]. In general, it has been recognized that this kind of experiments represent stringent test of the molecule-surface interaction. More precisely, both the angular and rotational state distributions are very sensitive to the details of the PES, its anisotropy[15] and corrugation[16,29], position and depth of the adsorption wells[21,26] and heights of the reaction barriers. For all these reasons, the study of angular and rotational state distributions of reflected molecules constitutes a matchless method to characterize the PES. The comparison between the results obtained with the PW91 and RPBE PESs as well as with available experimental data[22] for the N_2/W(110) system will allow us to gain a more detailed insight on the virtues and shortcomings of these two exchange-correlation functionals to study the scattering dynamics.

The paper is organized as follows: the main ingredients of our theoretical method are briefly described in section II. The results obtained with the two PESs for the non-reactive scattering dynamics of N_2 on W(110) are presented in section III, where we analyze and

compare the angular and rotational distributions of the reflected molecules obtained in each case. In section IV comparison with the experiments is performed and the quality of the two PESs in the different regimes is discussed. Finally, the main results of the work are summarized in section V.

II. THEORETICAL METHOD

The scattering of N_2 from the W(110) surface is simulated with pure 6D classical molecular dynamics calculations that neglect the initial zero point energy of the molecules[30]. The dependence of the scattering on the incidence conditions of the molecular beam (incidence energy E_i and polar angle Θ_i, typically) is determined using a conventional Monte Carlo sampling on the molecular orientation and position over the surface unit cell (see ref. 31 for more details). The results shown here for each incidence condition are obtained from a minimum of 20000 trajectories. The molecules are initially in the ground rotational state (J=0).

The final rotational state of the scattered molecules is determined by discretizing the classical angular momentum J_{cl} as imposed by the quantum angular momentum spectra. Thus, the rotational state J_f is assigned as the closest integer that verifies

$$J_f = \frac{-1 + \sqrt{1 + 4\,J_{cl}^2/\hbar^2}}{2} \tag{1}$$

This discretization procedure of the classical rotational spectra has been successfully applied to describe the rotational excitation of H_2 scattered from various metal surfaces[32]. Here, such an approximation is also well justified because the N_2 rotational constant is much smaller than that of H_2 [$B_e(N_2) = 1.998$ cm^{-1} and $B_e(H_2) = 60.85$ cm^{-1}][33]. The rotational constant is defined as $B_e = \hbar^2/(\mu r_0^2)$, where μ is the reduced mass and r_0 the bond length. For the sake of simplicity, we neglect the selection rules for rotational transitions related with the symmetry of the molecular wave function[34] when calculating the rotational distributions of section III, since our purpose is to compare the results obtained with the different functionals.

In order to analyze the dependence of the scattering properties on the XC functional, we use the 6D PESs of ref. 6 and refs. 31 and 35 that are calculated using the RPBE and the PW91 functionals, respectively. Details of the PES calculations can be found in those

references. Here we briefly describe the general procedure. The multi-dimensionality of the PES is reduced within the frozen surface approximation to a 6D function that only depends on the position $\mathbf{r}_i$ and $\mathbf{r}_j$ of the nitrogen atoms over the surface unit cell. The N_2/W(110) PES is constructed in each case from a set of 5610 DFT energies. In both cases, the corrugation reducing procedure[36] is used to interpolate the DFT data set and evaluate the energy at any position $\mathbf{r}_i$ and $\mathbf{r}_j$ of the N atoms. In general the RPBE PES is more repulsive than the PW91 one. As shown in ref. 6, the difference between the RPBE and PW91 energies for the same molecular configuration increases monotonously from tens of meV at $Z \sim 4$ Å to about 300 meV at $Z \sim 2.5$ Å, where Z is the distance of the molecular center of mass from the surface topmost layer. At smaller distances, there are configurations for which the energy difference can be as large as 500 meV. Here, a molecule configuration is defined by fixing the position of the molecular center of mass over the surface (X, Y), the internuclear distance, and the molecular orientation. In both PESs, the interaction of N_2 with the W(110) surface is characterized by a chemisorption well located at $Z \sim 2.6$ Å from the surface with a depth of 0.705 eV in the PW91 PES and 0.389 eV in the RPBE PES. As shown in refs. 6, 31, and 35, the chemisorption well plays an important role in the dissociative dynamics under normal incidence conditions and energies below 500 meV. The reason is that the molecules are first dynamically trapped around the well before dissociating. In this respect, two factors contribute to the different dissociation probabilities predicted by the two PESs: (i) the percentage of molecules reaching the well is slightly higher in the PW91 PES that is less repulsive than the RPBE and (ii) the path to dissociation from the bottom of the chemisorption well is 0.467 eV lower than the path to reflection in the PW91 PES, whereas the energy difference is only 0.145 eV in the RPBE PES. This last point explains that a large percentage of the trapped molecules dissociates in the PW91 but not in the RPBE. As a result the RPBE predicts dissociation probabilities smaller than 10^{-2} for incidence energies below 700 meV, whereas in the PW91 PES the dissociation probability is only negligible at energies below 50 meV.

III. COMPARISON OF THE PW91 AND RPBE NON-REACTIVE SCATTERING DYNAMICS

In this section we analyze the scattered N_2 molecules and compare their angular and rotational distributions obtained with the two PESs for normal incidence conditions ($\Theta_i = 0°$). All the distributions shown in this section are normalized to the unit area.

In order to understand the differences in the PW91 and RPBE distributions, we consider meaningful to focus on two characteristics of the PESs: (i) their Z dependence and (ii) their dependence on the molecular orientation, internuclear distance, and position over the surface unit cell (henceforth, denoted as PES corrugation). The reason is that Z is the leading variable in the entrance channel, i.e., at large distances from the surface where the molecule-surface interaction is still weak. In contrast, the PES corrugation leads the energy exchange from the perpendicular to the parallel and internal degrees of freedom. The analysis performed for the dissociation process in ref. 6 shows that the differences obtained with the two PESs are partially due to the different Z dependence. The conclusion extracted is that the PW91 is more accurate to describe the entrance channel, whereas the chemisorption and dissociation energies are better represented with the RPBE PES. Our purpose here is to confirm that finding and to extract information on the validity of each PES regarding the other degrees of freedom. We start by comparing these two properties between both PESs (Z dependence and PES corrugation) using the dynamics to filter out the relevant part of the 6D configuration space.

The distribution of the closest approach distances $Z_{\min}$ provides direct information on the Z-regions that are explored by the reflected molecules. Figure 1 shows the $Z_{\min}$ distributions obtained with both functionals at normal incidence and various incidence energies E_i that are representative of the different situations we can find in the scattering dynamics. As expected, the general trend in both calculations is that the molecules explore closer distances to the surface when increasing E_i. At energies above 0.75 eV, the RPBE and the PW91 $Z_{\min}$ distributions are very similar. The molecules have enough energy to overcome all the energy barriers in the entrance channel and are reflected close to the surface, in most cases at distances well below the chemisorption well position ($Z \sim 2.6$ Å). By analyzing this energy range we can extract information on the differences between both PESs regarding the dependence on the molecular orientation, internuclear distance, and position over the

surface unit cell.

For lower energies ($E_i < 0.75$ eV), the PW91 and RPBE $Z_{\min}$ distributions differ significantly. In this energy range, the scattering dynamics performed in both PESs is characterized by two kind of trajectories, the molecules that are reflected by the energy barriers in the entrance channel and the molecules that pass the entrance channel and are dynamically trapped around the chemisorption well before being reflected. The former kind of trajectories are identified with maxima at $Z > 2.6$ Å and the latter with maxima at $Z < 2.6$ Å in the $Z_{\min}$ distributions. We observe that for $E_i = 0.1$ eV all the molecules are reflected in the entrance channel with the RPBE, whereas about 20% of the molecules can already overcome the barriers with the PW91. The more repulsive nature of the RPBE PES is clearly confirmed when comparing the results for $E_i = 0.5$ eV. At this incidence energy, half of the configurations are still reflected in the entrance channel with the RPBE, whereas almost all the molecules can overcome the energy barriers at the entrance with the PW91. The results obtained at low energies ($E_i < 0.75$ eV) provide direct information about the differences on the magnitude of the energy barriers and on the distances at which those barriers are located in each PES. The existence of two well-defined regions where the molecules are reflected resembles the *dual-repulsive wall* model proposed in ref. 37 to explain the non reactive scattering of O_2 from Ag(111).

Together with the Z dependence, the PES corrugation is the property that determines the gas/surface dynamics. The concept of corrugation in this context refers to the dependence of the potential energy on the molecular orientation, internuclear distance and position over the surface unit cell. In order to quantify the PES corrugation at a given distance Z one can calculate the statistical standard deviation of the potential energy for all possible molecular internal degrees of freedom and positions over the surface unit cell. However, in doing so one is including configurations that are not accessible and, therefore, relevant in the gas/surface dynamics. For this reason we prefer to calculate the standard deviation only including those configurations that are probed by the molecules in the dynamics. More precisely, we define the standard deviation $\sigma(Z, E_i)$ of the potential energy of the molecules with incident energy E_i reaching the distance Z as follows:

$$\sigma(Z, E_i) = \sqrt{\frac{1}{N(Z, E_i) - 1} \sum_{j=1}^{N(Z,E_i)} \left[V_j(Z, E_i) - \overline{V}(Z, E_i)\right]^2}. \qquad (2)$$

In this expression $V_j(Z, E_i)$ is the potential energy of molecule j with incident energy E_i when

it is at distance Z from the surface, $N(Z, E_i)$ is the total number of molecules with energy E_i that reach Z, and $\overline{V}(Z, E_i)$ is the average of $V_j(Z, E_i)$ over all $N(Z, E_i)$. The results obtained with both PESs are shown in Fig. 2 for the incidence energies discussed above (E_i = 0.1, 0.5, 1.0, 1.7 eV). For each E_i, the standard deviation is only calculated at the distances that are probed by a large percentage of the reflected molecules ($N(Z, E_i) > 50\%$), otherwise the value of $\sigma(Z, E_i)$ is meaningless. As expected for corrugated PESs, $\sigma(Z, E_i)$ increases with increasing E_i, since higher energy molecules are able to explore wider regions of the configuration space. Additionally, the increase of $\sigma(Z, E_i)$ at small Z values reflects the larger corrugation close to the surface. The figure shows that the PW91 PES is more corrugated than the RPBE. As seen below, the latter has important implications regarding the differences obtained with the two PES in the angular and rotational state distributions of the reflected molecules.

In general, the specularity of the scattering angle distributions is obtained in an ideal elastic collision with a potential that only depends on Z. Off-specularity and broad angular distributions are associated to corrugated PESs. In Fig. 3 we show the final polar angle distributions of all the scattered molecules, i.e, we collect all the molecules reflected at Θ_f for all the outgoing azimuthal angles. The final polar angle Θ_f is measured respect to the surface normal. For E_i = 0.1 eV, the RPBE distribution is sharply peaked at the specular angle. The reason is that the molecules are reflected far from the surface, at distances larger than 3.5 Å, where the PES corrugation is low as indicated by the negligible values of σ (see Fig. 2). The PW91 distribution is broader and less specular. In this PES there is a small percentage of molecules reflecting rather close to the surface, in the region of the chemisorption well. However, we have verified that the shape of the distribution is unchanged even if only the molecules with the turning point above 3 Å are included. Thus, the obtained broadening demonstrates that the corrugation of the PW91 PES is already important at these large distances from the surface. Figure 2 shows that the standard deviation in this case is about 50 meV. This value is not negligible when compared with the 0.1 eV of incident energy.

For E_i = 0.5 eV, the two angular distributions are very similar. This result is surprising for two reasons: first, the molecules are probing different surface regions with each PES and second, the standard deviation is a factor of two larger for the PW91 than for the RPBE at distances below 2.5 Å. A detailed analysis of the angular distributions shows that the

width of the PW91 distribution is caused by the PES corrugation in the region where the chemisorption well is located. In contrast, the shape of the RPBE distribution is masking the two kind of trajectories mentioned above: the molecules that are reflected in the entrance channel before reaching the chemisorption well ($Z > 2.5$ Å, full line) and those reflected in the chemisorption well region (dashed line). As for the PW91, we observe that the broadening is due to the PES corrugation around the well. On the contrary, the maximum, which is closer to the specular angle in the RPBE calculation, is due to the molecules reflected in the entrance channel. Hence, the agreement of the two angular distributions under these incidence conditions is fortuitous and, by no means, indicates an equal description of the molecule-surface interaction by the two PESs.

For $E_i > 0.75$ eV, the differences obtained in the angular distributions provide a more direct information on the different characteristics of the two PESs, since the scattered molecules probe the same surface regions in both cases, i. e. distances below 2.2 Å as seen in Fig. 1. In this respect, the broader distributions obtained with the PW91 PES in this energy range show that this PES is more corrugated than the RPBE one also in this region. This conclusion is in accordance with the calculated values of σ for $E_i = 1.0$ and 1.7 eV at $Z \lesssim 2.2$ Å.

Compared with the low energy regime, the PW91 distributions for $E_i = 1.0$ and 1.7 eV and the RPBE distribution for $E_i = 1.7$ eV exhibit a double peak structure that deserves further analysis. We find that such structure is related with a large increase of the PES corrugation at distances from the surface lower than 2 Å. In order to illustrate this statement, the angular distributions are represented in Fig. 4 as the sum of two contributions: the distribution of the molecules reflecting above 2 Å (full lines) and the distribution of those that reflect below that distance (dash-dotted lines). In general, the distributions are quite specular when the molecules reflect above 2 Å and they are shifted to higher angles for the molecules that get closer to the surface. Note also that the idea of an increase of corrugation at $Z \sim 2$ Å is in agreement with the σ values shown in Fig. 2 for both PESs at $E_i = 1.7$ eV and also for the PW91 at $E_i = 1.0$ eV. In this figure, we also observe that the standard deviation of the RPBE PES for $E_i = 1.0$ eV remains almost constant in the interval of distances below 2 Å. This fact explains the absence of the double peak structure in this particular case.

Additional information can be obtained from the final rotational state distributions of the

scattered molecules. In Fig. 5 we show these distributions for normal incident molecules. As a general trend, the molecules are excited to higher rotational states as E_i increases. Furthermore, the distributions get broader with increasing E_i because the molecules probe the more corrugated regions at close distances from the surface. Focusing now in the differences between both simulations, we observe that the PW91 distributions are typically broader and peak at higher values of the rotational quantum number J than the RPBE ones. The discrepancy is particularly important for $E_i = 0.1$ eV. Here, the RPBE predicts a rotationally cold distribution ($J < 4$) that is at variance with the broad PW91 curve. The differences between the PW91 and RPBE distributions gradually vanish as the incidence energy increases. These results are consistent with the conclusions extracted from the angular distributions that points to the more repulsive character of the RPBE PES and the larger corrugation of the PW91 one.

We have also calculated the scattering at different incident angles as shown in Fig. 6. In general, the conclusions extracted from the comparison at normal incidence are also valid for off-normal incidence. The only distinction is that the value of 0.75 eV, which represents at normal incidence the energy threshold below which the rotational distributions given by the two PESs can significantly differ, increases with the incidence angle. The reason is that the perpendicular energy rules the distance of maximum approach. For instance at $\Theta_i = 30°$ the energy edge is at 1 eV and about 1.5 eV for $\Theta_i = 45°$.

IV. COMPARISON WITH THE EXPERIMENTS AND DISCUSSION

In the previous section we have observed appreciable differences between the results obtained with the two PESs for the angular and rotational state distributions of the scattered molecules. Since, in principle, no theoretical argument can be used to favor one functional above the other in order to judge the quality of the two PESs one is bound to perform comparisons with available experimental data.

The rotational state distribution of N_2 scattered from W(110) was measured in ref. 22 for various incident and detection conditions. The experiments were performed at a surface temperature of 1200 K. For this reason, we have first performed a few tests using the Generalized Langevin Oscillator model as implemented in refs. 38 and 39 and have verified that the width and shape of the rotational state distributions are not significantly different

from those obtained in our frozen surface calculations.

We start by comparing in Fig. 7 the final rotational state distributions obtained under normal incidence and detection conditions for different E_i. As in the previous section, all the distributions are normalized to the unit area. In agreement with the experimental data the width of both theoretical rotational distributions tend to increase with increasing incidence energy. Nevertheless, there exists a clear difference in the performance of each PES that depends on the incident energy. For energies below 0.75 eV, the PW91 distributions are in good agreement with the experimental data. Both the experiments and the PW91 PES results follow Boltzmann like distributions. This kind of behavior implies a corrugated PES that originates an almost random redistribution of the initial translational energy among the different degrees of freedom due to multiple scattering suffered by the molecule at the surface region. The agreement between the experimental and the PW91 distributions indicates that the molecule-surface repulsion is rather well described with this functional at distances from the surface larger than 2.0 Å. In contrast, the RPBE PES underestimates the amount of rotational excitation that is measured in the experiments for $E_i = 0.1$ and 0.5 eV. The results for 0.5 eV are particularly illustrative because revel differences between the two PESs that are masked in the polar angle distributions of Fig. 3. Here the small percentage of rotationally cold states (J$<$ 10) measured under these conditions confirms that the RPBE PES is unphysically too repulsive and/or not enough corrugated at large distances from the surface ($Z > 2.5$ Å).

For $E_i \geq 0.75$ eV, the RPBE distributions compare well with the experimental data. In fact, for $E_i = 1.0$ eV the RPBE distribution shows a better agreement with the experiments than the PW91 one. The latter is characterized by a sudden decrease of the highly excited rotational states, not observed experimentally. The departure from a Boltzmann like behavior is explained because under normal incidence and detection conditions the analyzed molecules are just the small percentage that is reflected above 2.0 Å [see Fig. 4 (a)]. In contrast, the molecules detected close to normal in the RPBE PES are reflected in a wider interval of distances. The conclusion extracted from the final polar angle and the rotational state distributions is that the PW91 is too corrugated at distances below 2.0 Å, since normal (i.e. quasispecular) reflection at these distances is unlikely. When compared with the experiments, this corrugation seems unrealistic.

As a complementary analysis, we provide in table I the rotational temperatures obtained

by fitting the rotational distributions to the following Boltzmann function,

$$P(\mathrm{J}, E_i) = P_0\,(2\mathrm{J}+1)\exp\left[-\mathrm{J}(\mathrm{J}+1)B_e/(K_B T_{rot})\right], \tag{3}$$

where J is the quantum rotational state, P_0 is a parameter and K_B is the Boltzmann constant. The rotational temperatures for $E_i = 0.1$ eV are the fits obtained for J>2. We note that the quality of the fit for the RPBE and PW91 distributions at $E_i = 0.5$ eV and $E_i = 1.0$ eV, respectively, is rather poor.

Additional information can be obtained looking at the rotational state distributions of molecules scattered at different detection angles. In Fig. 8 we compare the results obtained with the two PES and the experimental data of ref. 22 for two different angles of incidence ($\Theta_i = 0^\circ$ and $\Theta_i = 30^\circ$) and different outgoing angles. All measurements are done for an incidence energy of 0.5 eV. For each incident angle, the experimental rotational state distributions show no much dependence on the outgoing angle[40]. These results are rather well reproduced by the PW91 PES that, as discussed above, performs better at this energy. Note, however, that the PW91 distributions are slightly shifted to higher J-values than the experimental ones for $\Theta_i = 30^\circ$. In the case of the RPBE PES, the rotational state distributions at normal incidence shift to larger J values for subspecular reflection as compared to specular reflection. For $\Theta_i = 30^\circ$, we only show the results for quasispecular reflection because the number of molecules reflected within $\Theta_f = 50 \pm 2.5^\circ$ is negligible. All this is at variance with the experimental results, and another indication of the failure of the RPBE PES in the large distance region due to an excessive repulsion.

We have also analysed the vibrational state distributions of the reflected molecules. For $E_i \leq 1$ eV, the percentage of molecules reflected in an excited vibrational state is less than 1% both with the PW91 and the RPBE PESs. These results agree with the experimental observations[22] and do not provide information on the differences between both PESs.

V. SUMMARY AND OUTLOOK

In summary, we have performed a comparative analysis of the results obtained for the angular and rotational state distributions of N_2 molecules scattered from a W(110) surface using two different GGA functionals to construct the 6D PES. We observe that both functional provide a reasonable description of the rotational state distributions when comparing

with the experimental data. In particular, in agreement with the experiments, theoretical results show an increase of the width of the distributions and a shift of the distributions to higher J values when increasing the initial energy of the molecules.

Nevertheless, we have observed that there are also some differences on the results obtained with the two PES. In agreement with the study of the dissociative sticking coefficient[6] we observe that the RPBE PES is too repulsive at large distances from the surface. Additionally, in this study, looking at the final state of the scattered molecules, we observe that the PW91 PES is more corrugated, or in other words, it has a stronger dependence of the potential energy on the molecular orientation, internuclear distance, and position over the surface unit cell. This is reflected by the broader distributions obtained with this PES. Comparison with the experiments shows that the level of corrugation of the PW91 PES seems to be realistic for distances above the chemisorption well ($Z > 2.6$ Å). However, for high energy molecules ($E_i > 0.75$ eV) scattered closer to the surface the RPBE reproduces better the experimental results. The better performance of the RPBE (PW91) PES for $E_i > 0.75$ eV ($E_i < 0.75$ eV) is consistent with the results obtained for the dissociative adsorption[6].

Finally, we want to state that the overall agreement obtained with the experiments for such a sensitive quantity as the rotational distributions provides an important support for these dynamic simulation methods based on ab-initio DFT PESs. The differences obtained with the two PES and the different performances of each PES for different energies, establish, additionally, the level of accuracy that can be obtained in the simulations due to the unavoidable approximative nature of the exchange-correlation functional to be used within a DFT scheme. The performance of different exchange-correlation functionals in DFT is usually tested by comparison with available experimental information. In this respect, dynamical studies of elementary processes at surfaces provide a rich playground for such testing due to the multidimensional character of the problem. Otherwise said, regions of the configuration space with very different values of the electronic density are experimentally probed and an accurate description of electron exchange and correlation over all this density range is required. Dynamical studies like the one presented here should be thus helpful for methodological advance in DFT.

VI. ACKNOWLEDGEMENT

This work has been supported in part by the Basque Departamento de Educación, Universidades e Investigación, the University of the Basque Country UPV/EHU (Grant No. IT-366-07) and the Spanish Ministerio de Ciencia e Innovación (Grant No. FIS2010-19609-C02-02). Computational resources were provided by the DIPC computing center.

---

* sckkrang@ehu.es

† josebainaki.juaristi@ehu.es

‡ rdm@ehu.es

§ wapalocm@sq.ehu.es

[1] J. P. Perdew, J. A. Chevary, S. H. Vosko, K. A. Jackson, M. R. Pederson, D. J. Singh, and C. Fiolhais, Phys. Rev. B. **46**, 6671 (1992).

[2] B. Hammer, L. B. Hansen, and J. K. Nœrskov, Phys. Rev. B **59**, 7413 (1999).

[3] J. K. Vincent, R. A. Olsen, G. -J. Kroes, M. Luppi, and E. -J. Baerends, J. Chem. Phys. **122**, 044701 (2005).

[4] H. F. Busnengo and A. Martínez, J. Phys. Chem. C **112**, 5579 (2008).

[5] C. Díaz, E. Pijper, R. A. Olsen, H. F. Busnengo, D. J. Auerbach, and G. J. Kroes, Science **326**, 832 (2009).

[6] G. A. Bocan, R. Díez Muiño, M. Alducin, H. F. Busnengo, and A. Salin, J. Chem. Phys. **128**, 154704 (2008).

[7] J. I. Juaristi, M. Alducin, R. Díez Muiño, H. F. Busnengo, and A. Salin, Phys. Rev. Lett. **100**, 116102 (2008).

[8] H. E. Pfnür, C. T. Rettner, J. Lee, R. J. Madix, and D. J. Auerbach, J. Chem. Phys. **85**, 7452 (1986).

[9] C. T. Rettner, E. K. Schweizer, H. Stein, and D. J. Auerbach, Phys. Rev. Lett. **61**, 986 (1988).

[10] C. T. Rettner, H. Stein, and E. K. Schweizer, J. Chem. Phys. **89**, 3337 (1988).

[11] C. T. Rettner, E. K. Schweizer, H. Stein, and D. J. Auerbach, J. Vac. Sci. Technol. A **7**, 1863 (1989).

[12] C. T. Rettner, E. K. Schweizer, and H. Stein, J. Chem. Phys. **93**, 1442 (1990).

[13] M. Beutl, K. D. Rendulic, and G. R. Castro, Surf. Sci. **385**, 97 (1997).

[14] G. O. Sitz, A. C Kummel and R. N. Zare, J. Chem. Phys. **89** 2558 (1988).

[15] G. O. Sitz, A. C Kummel, R. N. Zare and J. C. Tully, J. Chem. Phys. **89** 2572 (1988).

[16] A. C Kummel, G. O. Sitz, R. N. Zare and J. C. Tully, J. Chem. Phys. **89** 6947 (1988).

[17] A. C Kummel, G. O. Sitz, R. N. Zare and J. C. Tully, J. Chem. Phys. **91** 5793 (1989).

[18] K. R. Lykke and B. D. Kay, J. Chem. Phys. **90**, 7602 (1989).

[19] K. R. Lykke and B. D. Kay, J. Chem. Phys. **92**, 2614 (1990).

[20] A. W. Kleyn and T. C. M. Horn, Phys. Rep. **199**, 192 (1991).

[21] K. R. Lykke and B. D. Kay, J. Phys.: Condens. Matter **3**, S65 (1991).

[22] T. F. Hanisco and A. C. Kummel, J. Vac. Sci. Technol.A **11** 1907 (1993).

[23] T. F. Hanisco and A. C. Kummel, J. Chem. Phys. **99** 7076 (1993).

[24] A. W. Kleyn, Surf. Rev. Lett. **1**, 157 (1994).

[25] J. L. W. Siders and G. O. Sitz, J. Chem. Phys. **101** 6264 (1994).

[26] A. E. Wiskerke and A. W. Kleyn, J. Phys.: Condens. Matter **7**, 5195 (1995).

[27] A. W. Kleyn, Prog. Surf. Sci. **54**, 407 (1997).

[28] C. M. Matthews, F. Balzer, A. J. Hallock, M. D. Ellison, and R. N. Zare, Surf. Sci. **460** 12 (2000).

[29] C. Díaz, F. Martín, H. F. Busnengo, and A. Salin, J. Chem. Phys. **120**, 321 (2004).

[30] In the PW91 PES, we also performed quasiclassical calculations that includes the initial zero point energy of the molecule (E_0=0.1423 eV) for all the incidence energies and angles shown in the present study, but we find no substantial differences in the final polar angle and rotational distributions obtained with both calculations (not even for E_i=0.1 eV).

[31] M. Alducin, R. Díez Muiño, H. F. Busnengo, and A. Salin, J. Chem. Phys. **125**, 144705 (2006).

[32] C. Díaz, H. F. Busnengo, F. Martín, and A. Salin, J. Chem. Phys. **118**, 2886 (2003).

[33] A. A. Radzig, B. M. Smirnov, *Reference Data on Atoms, Molecules and Ions* (Springer, Berlin, 1985).

[34] B. H. Bransden and C. J. Joachain, *Physics of Atoms and Molecules*, (Pearson Education, Essex, 2003).

[35] M. Alducin, R. Díez Muiño R, H. F. Busnengo, and A. Salin, Phys. Rev. Lett. **97**, 056102 (2006).

[36] H. F. Busnengo, A. Salin, and W. Dong, J. Chem. Phys. **112**, 7641 (2000).

[37] A. Raukema, R. J. Dirksen, and A. W. Kleyn, J. Chem. Phys. **103**, 6217 (1995).

[38] H. F. Busnengo, W. Dong, and A. Salin, Phys. Rev. Lett. **93**, 236103 (2004).

[39] H. F. Busnengo, M. A. Di Césare, W. Dong, and A. Salin, Phys. Rev. B **72**, 125411 (2005).

[40] In our calculations, we find that the distributions are only indistinguisable when the outgoing angles are close to the specular one ($\Theta_f \simeq \Theta_i \pm 15^\circ$). These are precisely the experimental conditions in ref. 22. However, we note that the distributions can differ for other outgoing angles.

TABLE I. Rotational temperatures obtained by fitting the rotational distributions of Fig. 7 to the Boltzmann function of Eq. (3). The experimental temperatures are from ref. 22. All temperatures are in Kelvin.

	E_i=0.1 eV	E_i=0.5 eV	E_i=0.75 eV	E_i=1.0 eV
PW91	130	1141	1262	1026
RPBE	59	496	1271	1267
Experiment	250	870±50	1130±60	1250±50

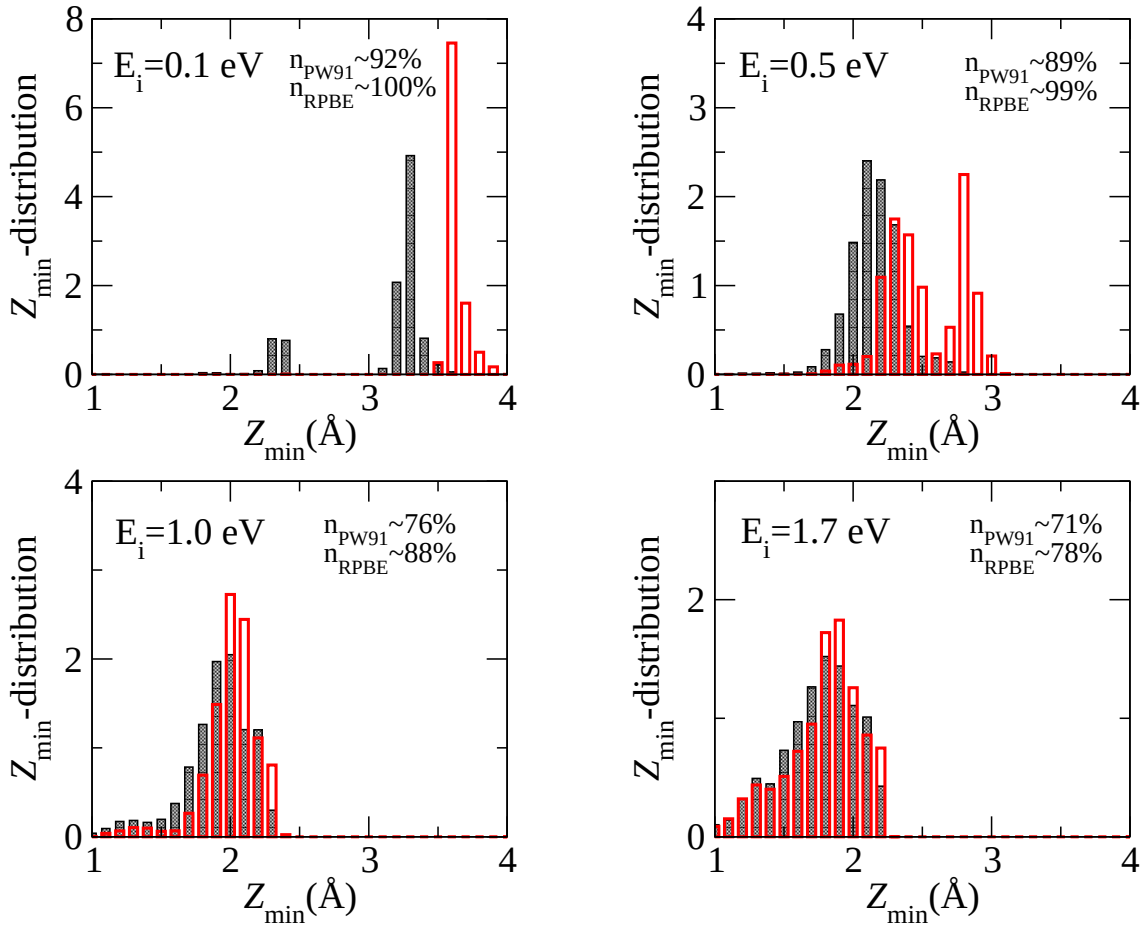

FIG. 1. (Color online) Closest approach distance distribution for all N_2 scattered from W(110) at normal incidence and at incidence energies E_i = 0.1, 0.5, 1.0, 1.7 eV. Shadowed (black) and open (red) bars show the results obtained with the PW91 and the RPBE, respectively. The bin is 0.1 Å in all panels. For each incidence energy, n_{RPBE} (n_{PW91}) shows the reflection probability obtained with the RPBE (PW91) PES.

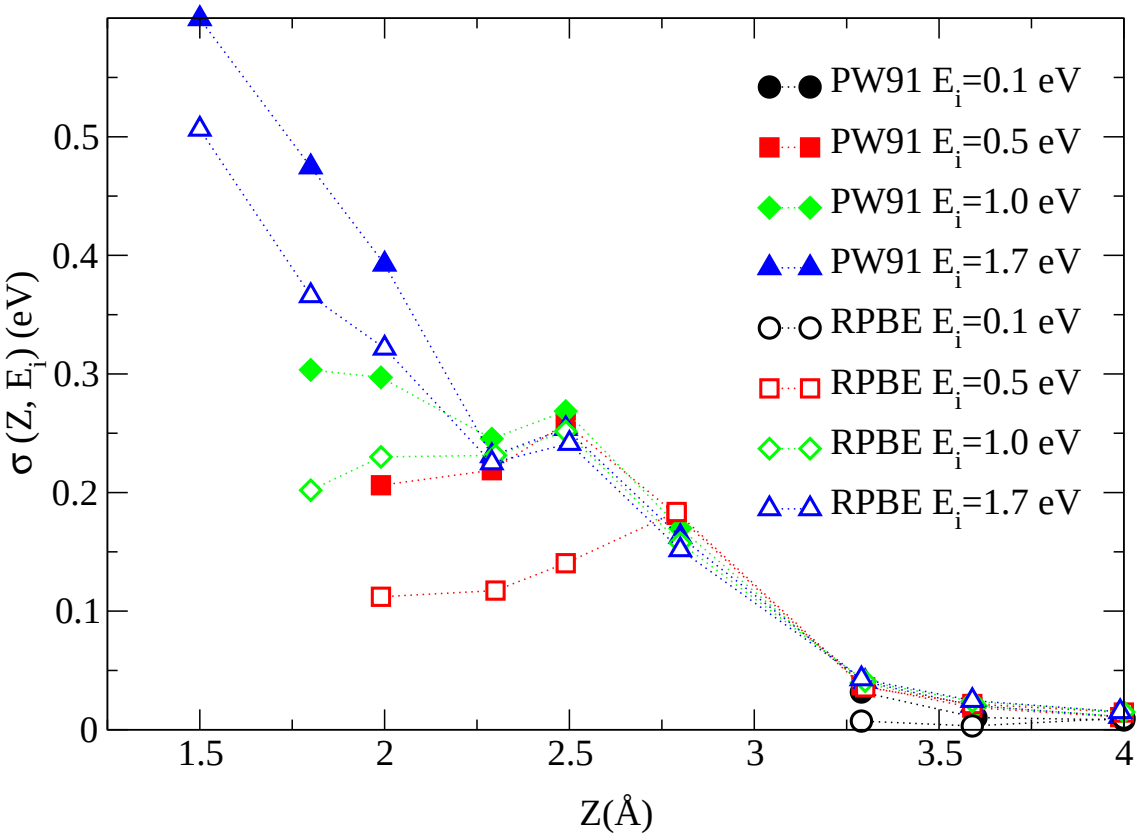

FIG. 2. (Color online) Standard deviation of the potential energy as a function of the distance from the surface Z. The deviation is calculated over the ensemble of molecules with incidence kinetic energy E_i that reach the distance Z [see Eq. (2)]. Filled (open) symbols show the deviation for the PW91 (RPBE) PES. Different symbols represent different E_i.

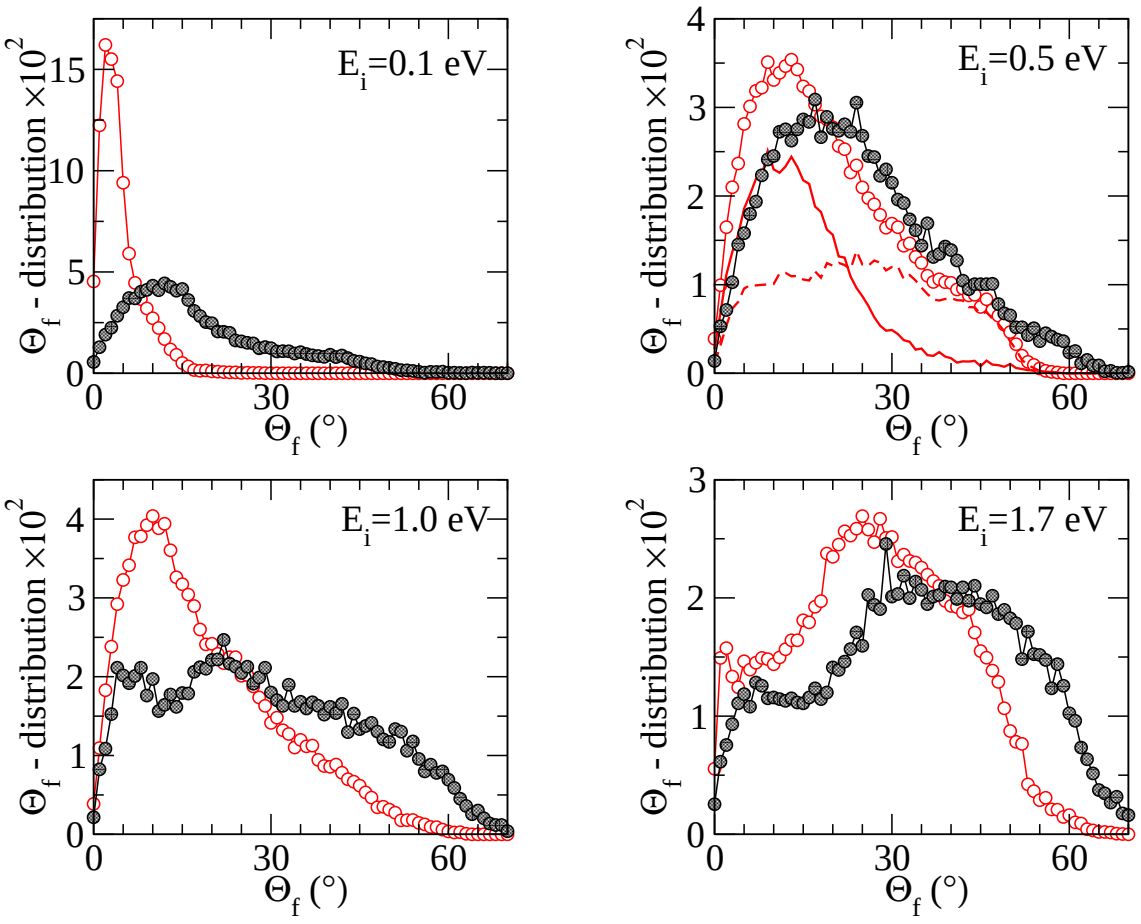

FIG. 3. (Color online) Comparison of the final polar angle distributions obtained with the PW91 (black shadowed circles) and the RPBE (red open circles) for N_2 scattered from W(110) at normal incidence and at various incidence energies. The bin is one degree. For $E_i = 0.5$ eV the full (dashed) line shows the RPBE angular distribution due to molecules reflected above (below) 2.5 Å.

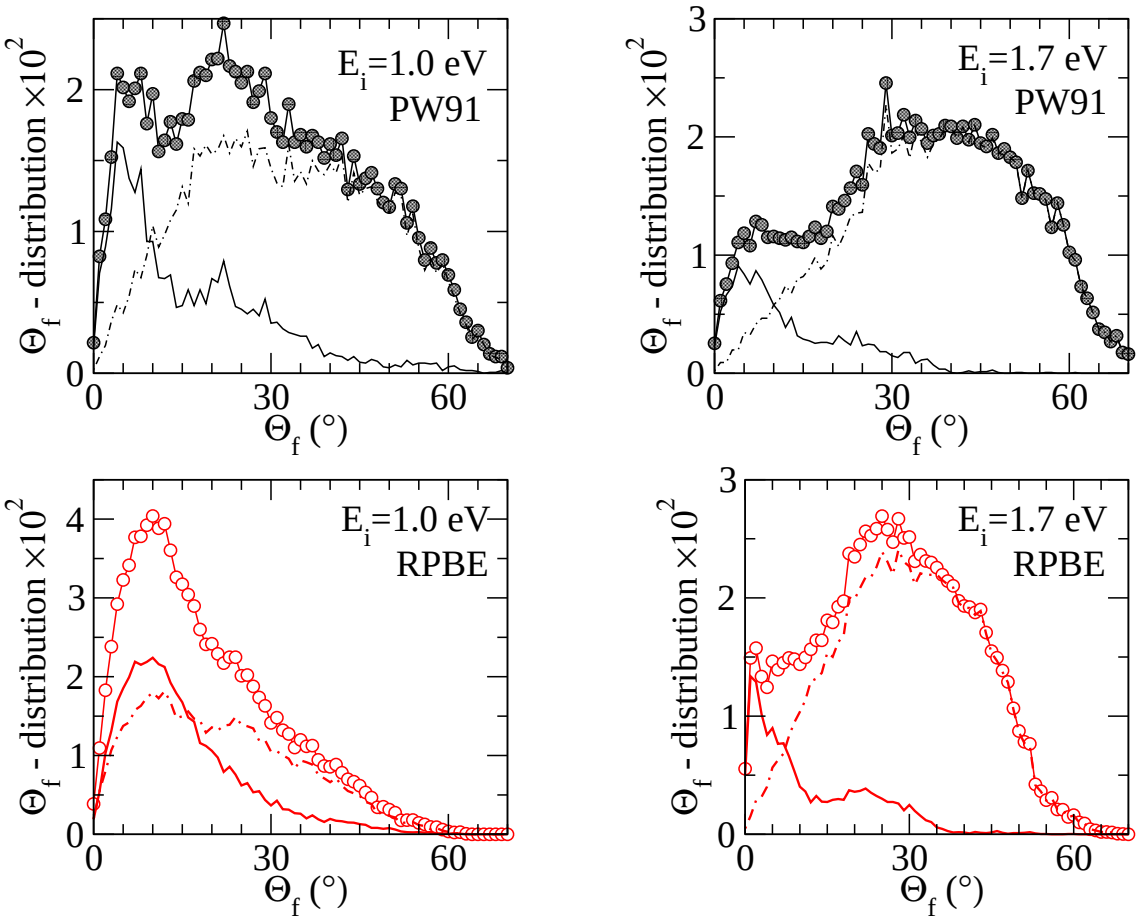

FIG. 4. (Color online) Contributions to the final polar angle distribution of the molecules reflecting above (full lines) and below (dash-dotted lines) 2.0 Å. The incidence energy and PES are written in each panel.

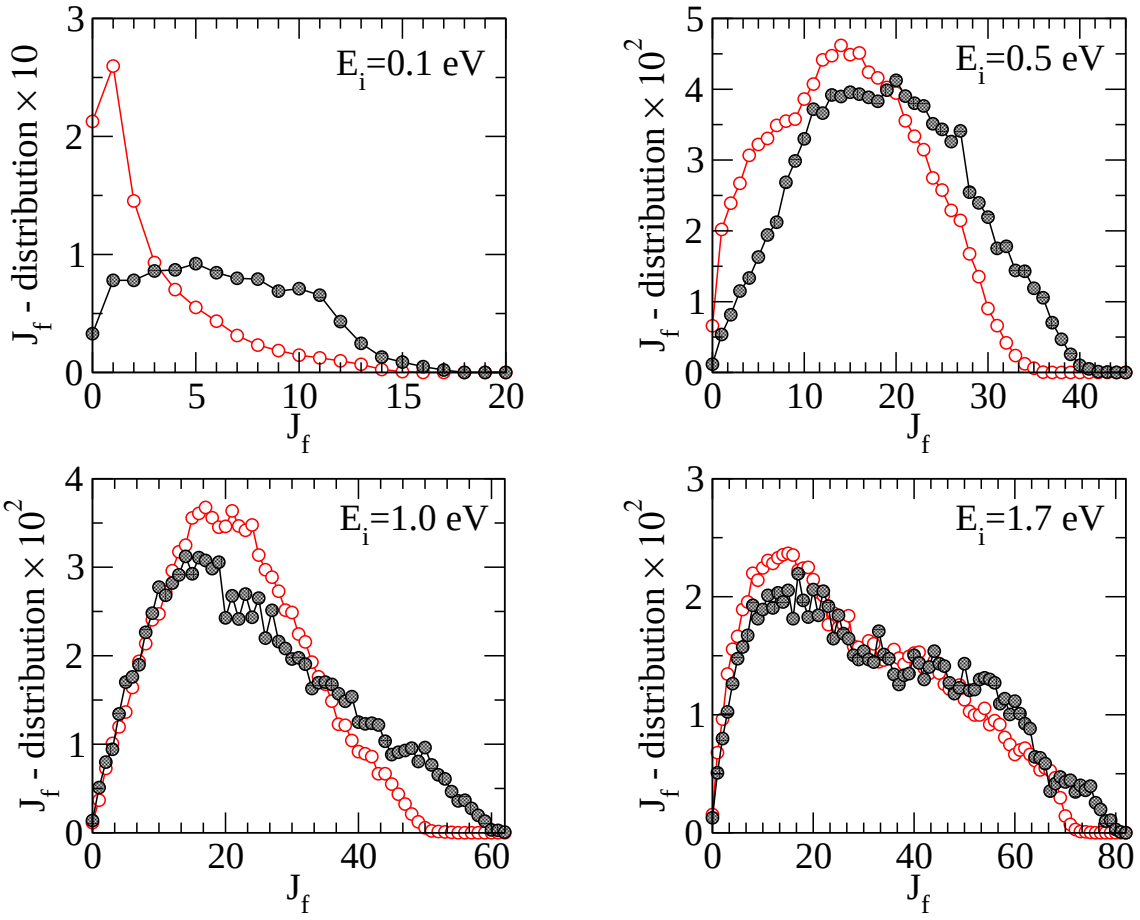

FIG. 5. (Color online) Comparison of the rotational state population distributions obtained with the PW91 (black shadowed circles) and the RPBE (red open circles) for N_2 scattered from W(110) at normal incidence and various incidence energies. Distributions are calculated for all the reflected molecules.

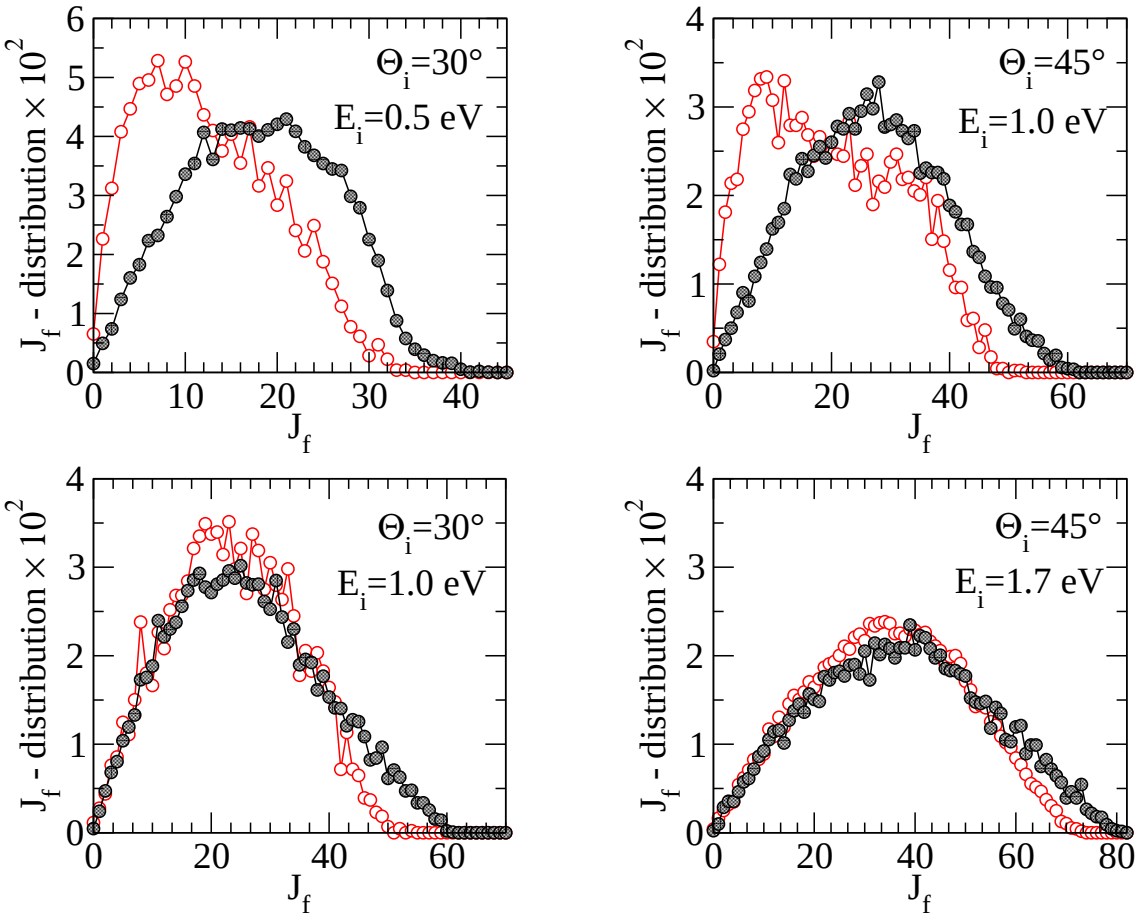

FIG. 6. (Color online) Same as Fig. 5 for off-normal incidence angles.

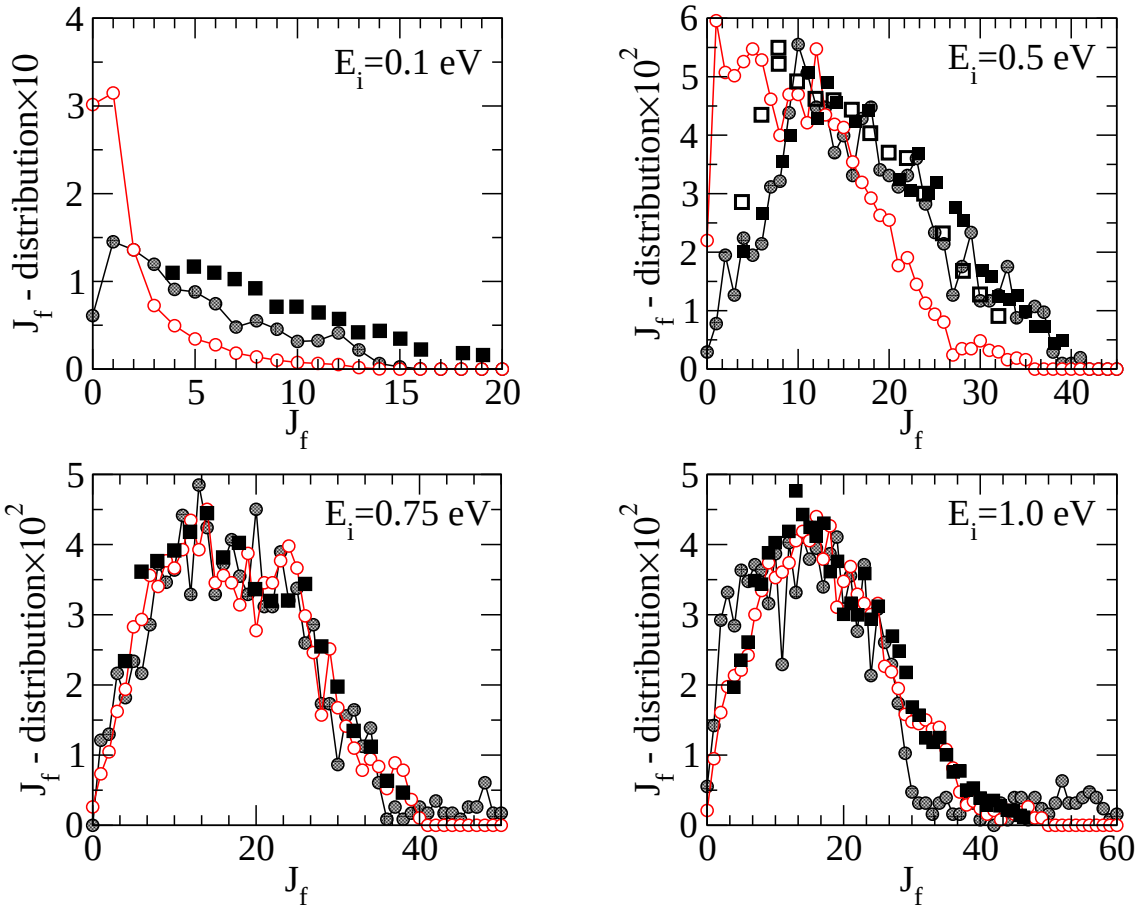

FIG. 7. (Color online) Rotational state population distributions for N_2 scattered from W(110) at normal incidence and detection angles ($\Theta_i = 0°$ and $\Theta_f < 5°$). The incidence energy is written in each panel. Results calculated with the PW91 (black shadowed circles) and the RPBE (red open circles) are compared with the experimental data of ref. 22 (empty and filled squares).

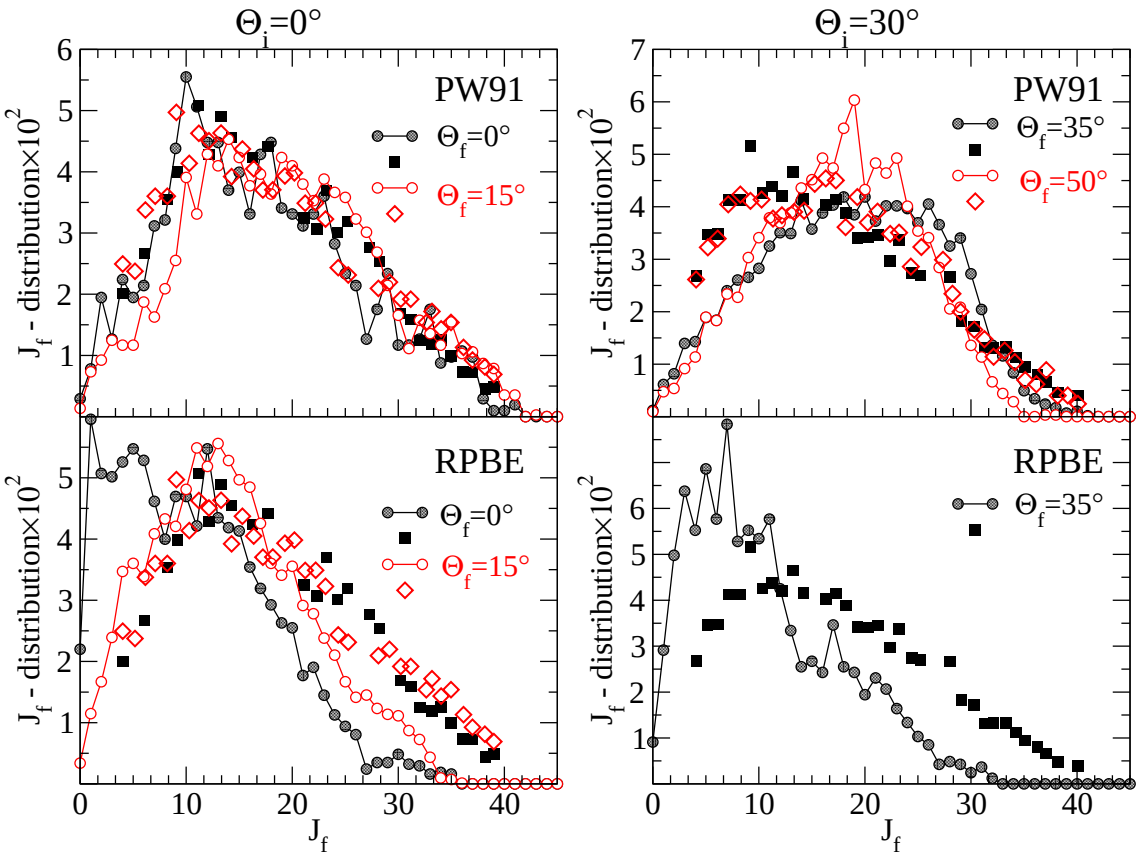

FIG. 8. (Color online) Rotational state population distributions for N_2 scattered from W(110) at normal incidence (left panels) and at $\Theta_i = 30°$ (right panels). The incidence energy is 0.5 eV. The experimental data of ref. 22 are compared with the PW91 results in the upper panels and with the RPBE ones in the lower panels. For normal incidence, the theoretical results for $\Theta_f = 0°$ and $\Theta_f = 15°$ are respectively shown by shadowed and open circles; and the experimental data by filled squares and open diamonds. At $\Theta_i = 30°$, the shadowed circles (filled squares) correspond to theoretical (experimental) distributions obtained at $\Theta_f = 35°$ and the open circles (open diamonds) to those obtained at $\Theta_f = 50°$. The RPBE results for $\Theta_f = 50°$ (not shown in the figure) are insufficient to assure a reliable statistics.